IEEE Access
Multidisciplinary | Rapid Review | Open Access Journal

Received 22 May 2023, accepted 15 June 2023, date of publication 27 June 2023, date of current version 3 July 2023.

Digital Object Identifier 10.1109/ACCESS.2023.3289837

APPLIED RESEARCH

Frequency Modulation Based on Hyperbolic Tangent Function for Position Closed Loop Control of Stepper Motor

WENLIN ZHOU, XIN LI, JUNZHANG QIAN, MO XIA, YI PU, PING JIANG, AND JINLONG HUANG

Institute of Optics and Electronics, Chinese Academy of Sciences, Chengdu 610209, China

Corresponding authors: Xin Li (lixin@ioe.ac.cn) and Jinlong Huang (huangjl@ioe.ac.cn)

This work was supported by the National Natural Science Foundation (NSFC) of China under Project 12293031.

ABSTRACT Generally, the position closed-loop control of stepper motors requires high-precision models, however stepper motors are complex nonlinear systems, and high-precision models are difficult to obtain. In order to solve this problem, a variable frequency controller based on hyperbolic tangent function is proposed. Similar to the proportional integral (PI) control method, this method does not require an exact model of the plant. The experimental results show that when tracking the sinusoidal signal $180^\circ \sin(0.628t)$, the tracking error of the Tanh control algorithm is reduced by nearly 60% compared with the PI control algorithm, which provides a new idea for the position closed-loop control of stepper motor.

INDEX TERMS Closed-loop control, stepper motor, hyperbolic tangent function, proportional integral (PI), pulse frequency control.

I. INTRODUCTION

The stepping motors [1], [2], [3] have the advantages of low cost, high power density, long service life and high reliability, so they are widely used in robot control and other fields [4], [5], [6]. Currently, stepper motor control technology and drive technology have also been studied and developed.

Li [7] proposed a robust control algorithm based on neural networks for stepper motor. In order to reduce the number of sensors and costs, Defoort [8] proposed a robust third-order sliding-mode controller for a stepper motor. Kim et al. [9] proposed a field-oriented control (FOC) control method that does not require direct axis and quadrature axis (DQ) transformation. Bendjedia [10] proposed a sensorless FOC control method. Kim et al. [11] proposed a nonlinear gain position control method that only requires position sensors. Kim and Ahn [12] and Li et al. [13] used active disturbance rejection control (ADRC) for motor control and achieved good results. Tran et al. [14] proposed an adaptive current controller based on neural network and double phase compensator. Le et al. [15] proposed an advanced closed-loop control to improve the performance of hybrid stepper motors. Lee et al. [16] proposed a nonlinear H_2 control for stepper motor control.

All of the aforementioned techniques need accurate models of stepper motors. However, due to the nonlinearity of stepper motors [17], obtaining an accurate model of a stepper motor is difficult [18], [19], [20], [21]. The traditional PI controller is widely used, but the control performances can not satisfy the requirements in some application. So a high performance none-model based control method is needed.

With the development of stepper motor micro-stepping drive technology [22], [23], [24], [25], [26], [27], [28], [29], common used stepper motor drivers are based on pulse frequency control, which do not require an accurate model of the motor and are easy to use. The typical control structure of a stepper motor is an open-loop control. A sequence of voltage pulses is fed to the motor to change the rest position with accurate steps. The last position is kept once the supply is disconnected [30]. Fig.1 shows the torque-frequency (torque-speed) characteristics of a stepper motor. According to the torque-frequency characteristics, it can be seen that the output

The associate editor coordinating the review of this manuscript and approving it for publication was Kan Liu.

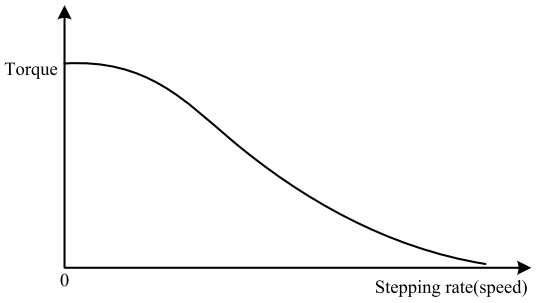

FIGURE 1. Pull-out torque characteristics of stepper motor.

torque of the stepper motor decreases with the increase of speed, so stepper motor will lose steps when the load is too large or the speed is too fast [31], [32], [33].

In order to improve the dynamic response of the stepper motor, Zhou et al. proposed a sine-type acceleration and deceleration method [34], and Wang et al. proposed a parabolic-type acceleration and deceleration method [35]. Comparing with the uniform acceleration and deceleration method, their dynamic characteristics are better, and are more in line with the torque-frequency characteristics of stepper motors. And the increase of position closed-loop can also prevent inaccurate positioning caused by step loss. However, the above methods are based on the total number of running steps for speed planning, and are not suitable for closed-loop position control based on position error. At present, the closed-loop control of stepper motors based on variable frequency is rarely studied.

In order to solve the position closed-loop control problem based on the variable frequency of stepper motor, this paper realizes the high-performance position control of a stepper motor without using the model. A tanh controller based on the hyperbolic tangent function is designed to control the input frequency and the direction signal of the motor driver, and the high-performance control of the stepper motor is realized. In order to verify the performance of the algorithm, the tanh controller is compared with the fuzzy controller and PI controller [36], [37], and the experimental results show that the tanh controller has faster convergence, higher position closed-loop accuracy and robustness.

This paper is organized as follows: In section II, the mathematical model of stepper motor is introduced. In section III, Tanh algorithm is proposed, and the stability is analyzed. Section IV provides the experimental results. The summary is drawn in Section V.

II. MATHEMATICAL MODEL OF STEPPER MOTOR

The mathematical model of two phases hybrid stepper motor is [1]:

$$\begin{aligned}
\dot{\theta} &= \omega \\
\dot{\omega} &= \frac{1}{J}\left[-K_m i_a \sin(p\theta) + K_m i_b \cos(p\theta) - B\omega - \tau_l\right] \\
\dot{i}_a &= \frac{1}{L}\left[v_a - Ri_a + K_m \omega \sin(p\theta)\right] \\
\dot{i}_b &= \frac{1}{L}\left[v_b - Ri_b - K_m \omega \cos(p\theta)\right]
\end{aligned} \tag{1}$$

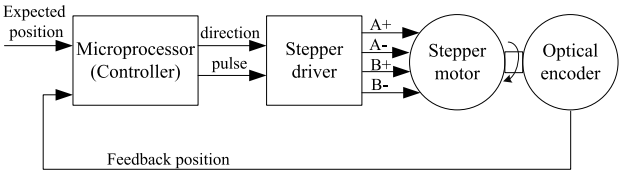

FIGURE 2. The structure of stepper motor control.

where i_a and i_b, v_a and v_b are the voltages and currents of phases A and B, respectively. θ is the rotor position, ω is the rotor velocity. B is the viscous friction coefficient. J is the inertia of the motor. K_m is the motor torque constant. R is the resistance of phase winding. L is the inductance of phase winding, and p is the number of rotor teeth. The load torque perturbation is τ_l.

From equation (1), it can be seen that the relationship between the output angle of the stepper motor and the input voltage is nonlinear. However, in actual engineering, the most common control method of stepper motor is controlled by PWM pulse frequency. The two-phase hybrid stepper motor is controlled by pulse frequency as shown in Fig.2.

The controller generates the corresponding PWM pulse and direction signal to the stepper motor driver according to the received instructions, and the stepper motor driver completes the current loop and micro-stepping control. For a stepper motor with n phases and p rotor teeth the step length is $2\pi/np$ and so the stepping rate is related to the rotor velocity by:

$$|\omega| = \frac{2\pi f}{np} \tag{2}$$

In which f is the stepping rate. When the micro-stepping of stepper motor drivers is N and the controller pulse frequency is f_{pwm}, the relationship between the motor output speed and the controller pulse frequency is:

$$|\omega| = \frac{2\pi f_{pwm}}{npN} \tag{3}$$

For two-phase hybrid stepper motors, constant current chopping and sinusoidal micro-stepping control are usually adopted. And if the number of micro-stepping is N, the step length of stepper motor become $1.8°/N$, so the larger N, the smaller each step of the stepper motor, and the higher the step resolution of the stepper motor. The value of micro-stepping N is binary or quinary, $N = 1, 2, 4, 5, 8, 10, 16, 20, 25, 32, 40, 50, 64, 100, 128, 200, 256, \cdots$, the value of N is chosen according to the actual demand.

Therefore, when the micro-stepping N is fixed, the rotation speed of the stepper motor can be controlled by controlling the pulse frequency f_{pwm}, and the differential f_{pwm} of is related to the acceleration of the motor. Changing the direction signal can change the direction of rotation of the motor.

III. DERIVATION OF TANH ALGORITHM

A. TANH CONTROLLER DESIGN

As we all know, $\tanh(x) = \frac{e^x - e^{-x}}{e^x + e^{-x}}$, and its first and second derivative of the function are shown in Fig.3. From Fig. 3,

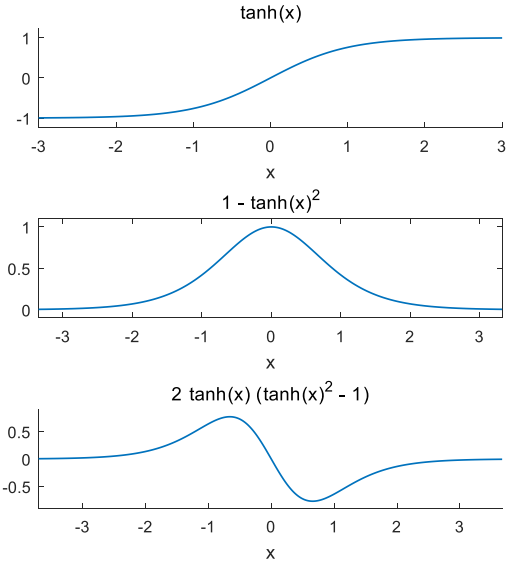

FIGURE 3. *tanh*(*x*) function and its derivatives.

we can see that $tanh(x)$ and its first and second derivatives are smooth and bounded. It is an odd fuction, we can get $\tanh(-x) = -\tanh(x)$. It has the following properties:

$$\tanh(x) = \begin{cases} 1, & x > 3.5 \\ x, & -0.3 < x < 0.3 \\ -1, & x < -3.5 \end{cases} \tag{4}$$

When $-3.5 < x < -0.3$ or $0.3 < x < 3.5$, the output of $tanh(x)$ is nonlinear. From (4) and Fig.3, we can see that if tanh function is used as the stepping rate controller, the output of the controller is smooth. According to the torque-frequency characteristics of the stepper motor, when the stepper motor starts, the starting frequency cannot be too high, otherwise the stepper motor will lose step. Therefore, the control frequency is gradually increased from the lower start-up frequency to a higher frequency. So the controller is divided into 3 segments: acceleration section, constant speed section, deceleration section. To achieve the maximum speed as quickly as possible, the acceleration section adopts uniform acceleration, and to reduce the oscillation and improve the positioning accuracy, the hyperbolic tangent function is adopted in the deceleration section. The controller is divided into 3 segments, the stepping rate closed-loop controller is:

$$f_{pwm}(k) = \begin{cases} f_{pwm}(k-1) + f_{up}, \\ \quad if \ \left(|e_\theta(k)| > e_0 \ and \ f_{pwm}(k-1) < f_{\max}\right); \\ f_{\max}, \\ \quad if \ \left(|e_\theta(k)| > e_0 \ and \ f_{pwm}(k-1) \geq f_{\max}\right); \\ f_{\max} \tanh\left(k_\omega |e_\theta(k)|\right), \\ \quad if \ \left(|e_\theta(k)| \leq e_0\right); \end{cases} \tag{5}$$

f_{pwm} is the input frequency of the motor driver, f_{max} is the maximum frequency of the motor, k_ω is the tuning parameter and $k_\omega > 0$, $e_\theta = \theta_{ref} - \theta$, θ_{ref} is the desired position, θ is the measurement position of encoder. f_{up} is the pulse frequency that increases during each control cycle of acceleration. e_0 is the deceleration zone, when the position error is less than the deceleration zone, the deceleration begins. Where $\tanh(x) = \frac{e^x - e^{-x}}{e^x + e^{-x}}$ is the hyperbolic tangent function.

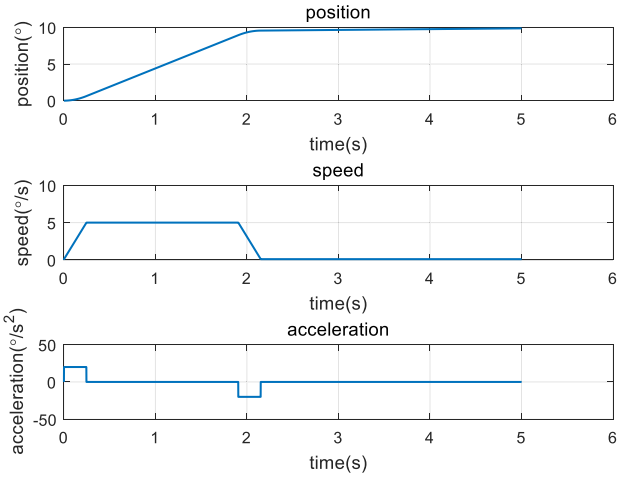

FIGURE 4. Uniform acceleration and deceleration method.

So the rotor velocity output is:

$$\omega(t) = \frac{2\pi f_{pwm}(t)}{npN} \operatorname{sign}(e_\theta(t)) \tag{6}$$

$\operatorname{sign}(e_\theta(t))$ is the sign of the position error.

$$sign(e_\theta(t)) = \begin{cases} 1, & if \ e_\theta(t) > 0 \\ -1, & if \ e_\theta(t) < 0 \end{cases} \tag{7}$$

It also represents the direction of angular velocity, so the position output is:

$$\theta(t) = \int_0^t \omega dt = \int_0^t \frac{2\pi f_{pwm}(t)}{npN} \operatorname{sign}(e_\theta(t))\, dt \tag{8}$$

The discrete form of $\theta(k)$ is:

$$\theta(k+1) = \tau \cdot \frac{2\pi f_{pwm}(k)}{npN} sign(e_\theta(k)) + \theta(k) \tag{9}$$

τ is the sampling period, usually $\tau \leq 0.001s$.

To illustrate the characteristics of the tanh controller, we compare it with the uniform acceleration and deceleration method. Fig.4 is the position, velocity and acceleration curve of the constant acceleration and deceleration method. Fig.5 is the position, velocity, and acceleration curves of the method in this paper. Comparing Fig.4 and Fig.5, it can be seen that the constant deceleration method has zero velocity when reaching the desired position, but the acceleration is not zero, jerk (differential of acceleration) will be infinity, and the motor will oscillate when it stops, and the position error increases. The tanh method changes smoothly in the deceleration section, and the jerk is smooth, which is more in line with the torque-frequency characteristics of the stepper motor. When the desired position is reached, the speed and acceleration are just zero, the jerk is zero, and the motor runs smoothly.

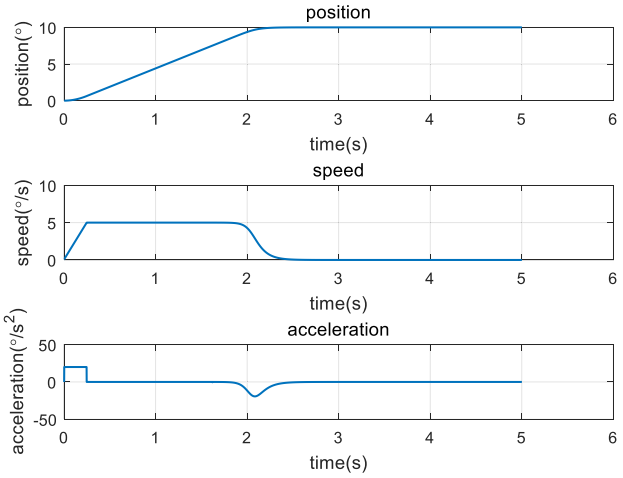

FIGURE 5. Tanh control method.

B. STABILITY ANALYSIS OF TANH

The Lyapunov function is designed as follows:

$$V(k) = \frac{1}{2}e_\theta^2(k) \tag{10}$$

When the position closed-loop control is stable, with $\lim_{k\to\infty} e_\theta(k) \to 0$, we need $\Delta V(k) = V(k+1) - V(k) < 0$, according to (9) and (10) :

$$\begin{aligned}
&\Delta V(k)\\
&= \frac{1}{2}e_\theta^2(k+1) - \frac{1}{2}e_\theta^2(k)\\
&= \frac{1}{2}\left(\theta_{ref} - \frac{2\pi f_{pwm}(k)}{npN}\tau \cdot sign(e_\theta(k)) - \theta(k)\right)^2\\
&\quad - \frac{1}{2}e_\theta^2(k)\\
&= \frac{1}{2}\left(e_\theta(k) - \frac{2\pi f_{pwm}(k)}{npN}\tau \cdot sign(e_\theta(k))\right)^2 - \frac{1}{2}e_\theta^2(k)\\
&= \frac{1}{2}e_\theta^2(k)\left(1 - \frac{2\pi f_{pwm}(k)}{npN \cdot e_\theta(k)}\tau \cdot sign(e_\theta(k))\right)^2 - \frac{1}{2}e_\theta^2(k)\\
&= \frac{1}{2}e_\theta^2(k)\left(-2\rho + \rho^2\right)
\end{aligned} \tag{11}$$

In which $\rho = \frac{2\pi f_{pwm}(k)}{npN \cdot e_\theta(k)}\tau \cdot sign(e_\theta(k))$. When $0 < \rho < 2$, we have $\Delta V(k) < 0$, $\lim_{k\to\infty} e_\theta(k) \to 0$.

According (5), we can get:

$$\rho = \begin{cases}
\dfrac{2\pi\left(f_{pwm}(k-1) + f_{up}\right)}{npN \cdot e_\theta(k)}\tau \cdot sign(e_\theta(k)),\\
\quad if\ \left(|e_\theta(k)| > e_0\ and\ f_{pwm}(k-1) < f_{\max}\right);\\
\dfrac{2\pi f_{\max}}{npN \cdot e_\theta(k)}\tau \cdot sign(e_\theta(k)),\\
\quad if\ \left(|e_\theta(k)| > e_0\ and\ f_{pwm}(k-1) \geq f_{\max}\right);\\
\dfrac{2\pi f_{\max}\tanh\left(k_\omega |e_\theta(k)|\right)}{npN \cdot e_\theta(k)}\tau \cdot sign(e_\theta(k)),\\
\quad if\ \left(|e_\theta(k)| \leq e_0\right);
\end{cases} \tag{12}$$

According (7), we have:

$$\frac{sign(e_\theta(k))}{e_\theta(k)} > 0, \quad e_\theta(k) \neq 0 \tag{13}$$

So if $k_\omega > 0$, we can get $\rho > 0$.
According (3), we know that:

$$\omega_{\max} = \frac{2\pi f_{\max}}{npN} \tag{14}$$

Bring (13) and (14) into ρ:

$$\rho = \begin{cases}
\dfrac{2\pi\left(f_{pwm}(k-1) + f_{up}\right)}{npN \cdot e_\theta(k)}\tau \cdot sign(e_\theta(k)),\\
\quad if\ \left(|e_\theta(k)| > e_0 and f_{pwm}(k-1) < f_{\max}\right);\\
\dfrac{\omega_{\max}}{e_\theta(k)}\tau \cdot sign(e_\theta(k)),\\
\quad if\ \left(|e_\theta(k)| > e_0\ and\ f_{pwm}(k-1) \geq f_{\max}\right);\\
\dfrac{\omega_{\max}\tanh\left(k_\omega |e_\theta(k)|\right)}{e_\theta(k)}\tau \cdot sign(e_\theta(k)),\\
\quad if\ \left(|e_\theta(k)| \leq e_0\right);
\end{cases} \tag{15}$$

Further:

$$\rho < \begin{cases}
\dfrac{\omega_{\max}\tau}{|e_\theta(k)|}, & |e_\theta(k)| \geq e_0\\
\dfrac{\omega_{\max}\tanh\left(k_\omega |e_\theta(k)|\right)}{|e_\theta(k)|} \cdot \tau, & if\ \left(|e_\theta(k)| \leq e_0\right)
\end{cases} \tag{16}$$

According (4), we have that:

$$\tanh\left(k_\omega |e_\theta(k)|\right) = \begin{cases}
1, & k_\omega |e_\theta(k)| > 3.5\\
k_\omega |e_\theta(k)|, & k_\omega |e_\theta(k)| < 0.3\\
0, & k_\omega |e_\theta(k)| = 0
\end{cases} \tag{17}$$

Thus, (16) can be further simplified to:

$$\rho < \begin{cases}
\dfrac{\omega_{\max}\tau}{e_0}\\
k_\omega \omega_{\max}\tau
\end{cases} \tag{18}$$

When:

$$e_0 > \frac{\omega_{\max}\tau}{2} \tag{19}$$

And:

$$0 < k_\omega < \frac{2}{\omega_{\max}\tau} \tag{20}$$

$0 < \rho < 2$ is satisfied, so the stability of the system can be guaranteed.

C. PARAMETER TURNING METHOD

In order to ensure the smooth of the output frequency f_{pwm} under different position error e_θ, according (5), we need:

$$f_{\max}\tanh\left(k_\omega \cdot e_0\right) = f_{\max} \tag{21}$$

However $\tanh(3.5) \approx 1$, so k_ω can be calculated according to the e_0.

$$k_\omega = \frac{3.5}{e_0} \tag{22}$$

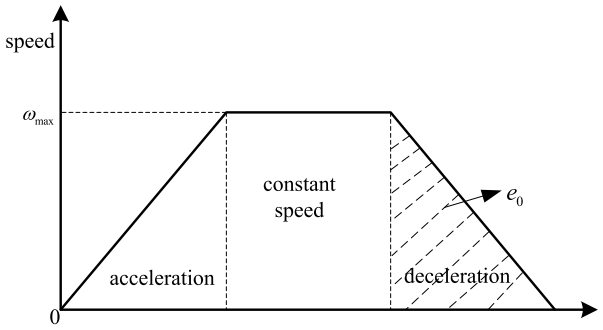

FIGURE 6. Uniform acceleration and deceleration.

The deceleration zone e_0 is related to the maximum speed of the motor $\omega_{\max}$ and the maximum acceleration $a_{\max}$. In order to obtain the value of deceleration zone e_0, we can derive it by the uniform acceleration and deceleration method, as shown in Fig.6, the area of the shadowed part is the value of e_0, and the derivation can be seen:

$$e_0 = \frac{\omega_{\max}^2}{2a_{\max}} \tag{23}$$

At any speed the maximum permissible acceleration is given by the equation:

$$Acceleration = (motor\ torque - load\ torque)\ /inertia \tag{24}$$

If the maximum torque of the motor, load torque and total inertia are known, we can calculate the maximum acceleration from these parameters.

The tuning parameters e_0 and k_ω can be calculated according to the maximum speed of the motor $\omega_{\max}$ and the maximum acceleration $a_{\max}$:

$$e_0 \approx \frac{\omega_{\max}^2}{2a_{\max}} \tag{25}$$

$$k_\omega \approx \frac{7a_{\max}}{\omega_{\max}^2} \tag{26}$$

Therefore, the adjustable parameters e_0 and k_ω are set according to the actual requirements.

IV. EXPERIMENT

A. EXPERIMENT AND PARAMETERS SETUP

The experiment setup is shown in Fig.7. The isolated power, control unit and motor driver are installed inside the box. The control unit is a DSP TMS320F28379D based board, which completes the encoder data acquisition, position loop calculation. The operation frequency of position loop is 1kHz. An position encoder is installed at ends of the motor axis, and the resolution is 4000PPR(pulse per revolution), the encoder resolution is 0.09°. The data recorded by the host computer and the recording frequency is 100Hz. The stepper motor is two phases hybrid stepper motor, the model name of the stepper motor is AM23HS3454, encoder model is E1000D. The parameters of the stepper motor are shown in Table 1.

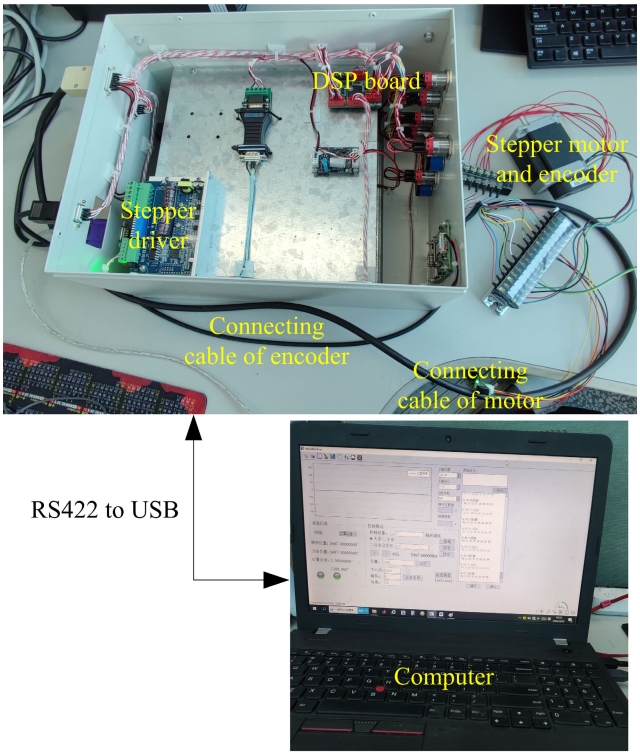

FIGURE 7. Experimental setup.

TABLE 1. Parameters of the stepper motor.

Symbol	Quantity	Values
I_p	Phase current	2.2A
J_m	Motor inertia	$4.6 \times 10^{-5} kg \cdot m^2$
p	Pole number	50
R_m	Resistance	$2.9\Omega/phase$
θ_s	Step length	1.8°
$T_{\max}$	Maximum peak static torque	$1.8N \cdot m$

In this experiment, a fuzzy control, proportional integral (PI) control and tanh control are tested respectively. The parameters of PI are $k_p = 200$, $k_i = 20$. The separation value is $e_0 = 6.66°$. The parameters of Tanh are $k_\omega = 0.52$. Other parameters are the same $f_{up} = 50$, $\omega_{\max} = 216°/s$. Stepper motor driver current is $I = 1.0A$, micro-stepping $N = 200$. Therefore, it can be calculated that the stepper motor will rotate $\frac{1.8°}{N} = \frac{1.8°}{200} = 0.009°$ degrees for each pulse received. So the angular resolution of stepper motors is 0.009°. The position sampling period is $\tau = 1 \times 10^{-3} s$.

B. EXPERIMENT RESULTS

1) SINUSOIDAL SIGNAL TRACKING TEST

In order to test the performance of the algorithm, we chose different sinusoidal signals to track according to the maximum speed. In this experiment, when the reference signal is $\theta_{ref} = 45° \sin(0.0628t)$, the maximum speed of tracking signal is $2.826°/s$, the results are shown in Fig.8 and table 2. When the reference signal is $\theta_{ref} = 180° \sin(0.314t)$, the

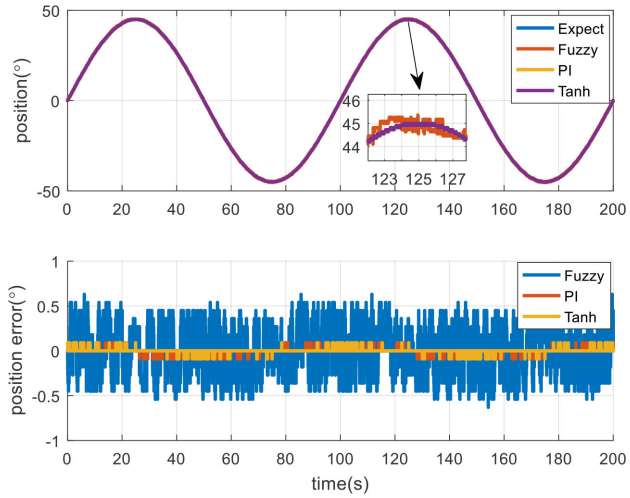

FIGURE 8. $\theta_{ref} = 45° \sin(0.0628t)$.

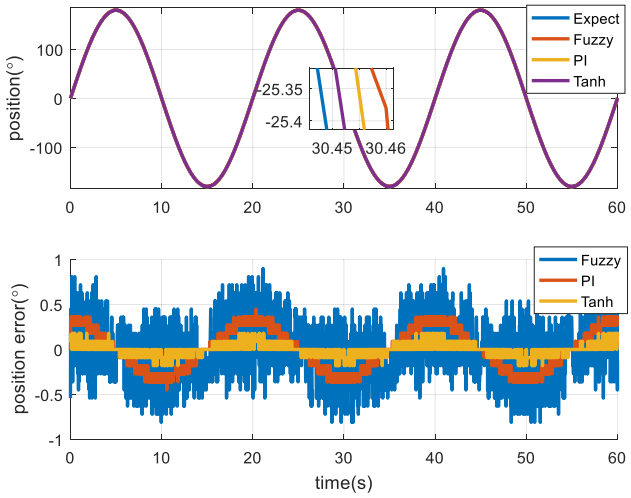

FIGURE 9. $\theta_{ref} = 180° \sin(0.314t)$.

TABLE 2. Position error comparision.

θ_{ref}	Fuzzy		PI		Tanh	
	PV	RMS	PV	RMS	PV	RMS
$y = 45° \sin(0.0628t)$	1.26	0.26	0.18	0.01	0.18	0.01
$y = 180° \sin(0.314t)$	1.71	0.31	0.90	0.22	0.36	0.07
$y = 180° \sin(0.628t)$	2.16	0.39	1.62	0.48	0.72	0.15

PV stands for peak to peak value, RMS stands for root mean square. The unit is degree.

maximum speed of tracking signal is $56.25°/s$, the results are shown in Fig.9 and table 2. When the reference signal is $\theta_{ref} = 180° \sin(0.628t)$, the maximum speed of tracking signal is $113.04°/s$, the results are shown in Fig. 10 and Table 2.

We can see that the tracking error is reduced by using tanh control method.

It can be concluded that, by using the tanh controller, when tracking low-speed sinusoidal signal $45° \sin(0.0628t)$,

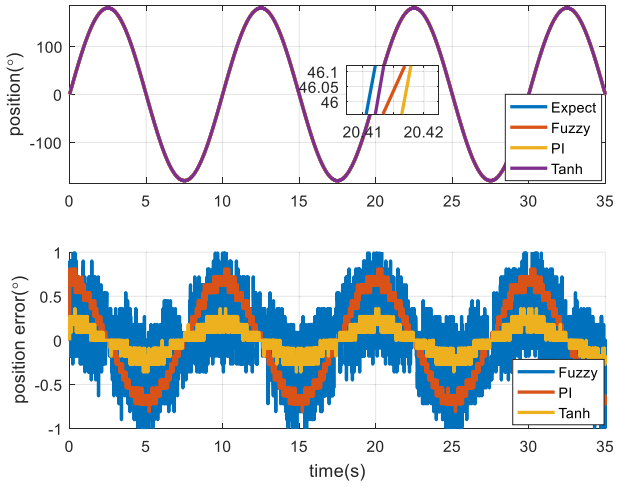

FIGURE 10. $\theta_{ref} = 180° \sin(0.628t)$.

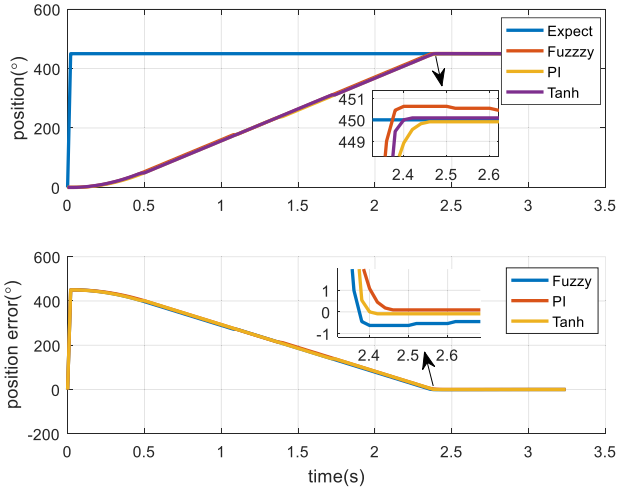

FIGURE 11. Step signal tracking 0° *to* 450° results.

the control performance of the PI controller and the tanh controller is not much different. However, when tracking the faster sinusoidal signal $180° \sin(0.628t)$, the control performance of the tanh controller is better than that of the PI controller, the PV error is reduced by 55% and the RMS error is reduced by 60%.

2) STEP SIGNAL TRACKING TEST

Step signal tracking results are shown in Fig.11 and Fig.12. The step response results show that although the response of the tanh controller is not as fast as that of the fuzzy controller, it does not have overshoot and stabilizes faster. The PI controller also doesn't have overshoot, but responds more slowly than the tanh controller.

3) STEP SIGNAL TRACKING TEST WITH DISTURBANCE

Different from other types of motors, stepper motors still have a holding torque when stop rotating if they are powered on, so stepper motors have an innate anti-disturbance ability.

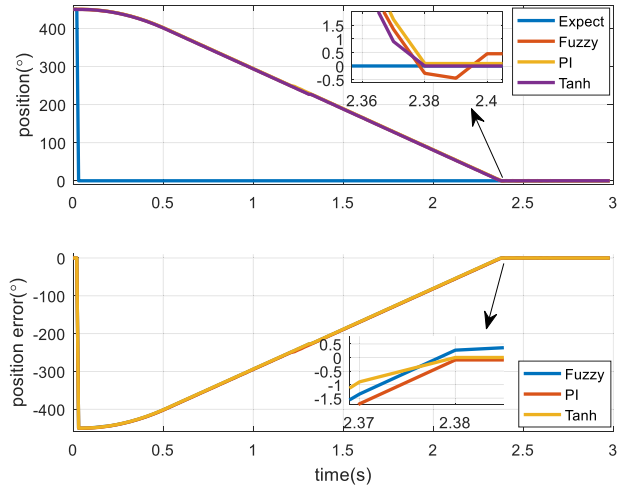

FIGURE 12. Step signal tracking 450° *to* 0° results.

TABLE 3. Parameters of current.

	Operation current	Holding current
Motor1	$1A$	$0.5A$
Motor2	$1.6A$	$0.3A$

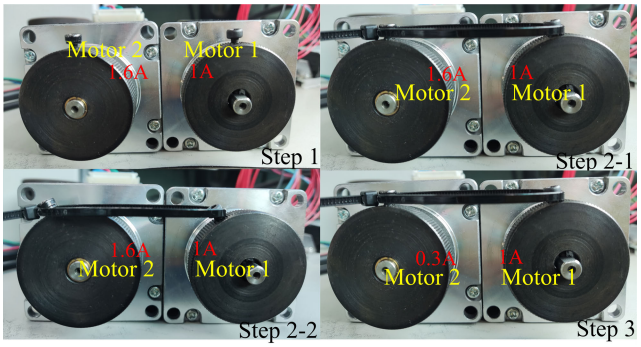

FIGURE 13. Experiment procedures.

The holding torque of a stepper motor is determined by the holding current. The larger the holding current, the greater the holding torque. However, the holding current should not be too large, because it will cause the motor coil to heat up and the temperature of the motor to rise.

In order to test the robustness of the algorithm, as shown in Fig.13, Motor2 is used as a load, and a "disturbance" is added by changing the output torque of Motor2. The current of the stepper motor are shown in Table 3.

The test procedures are:

Step 1: The initial position of Motor 1 is 0°, and the desired position is set to 360°. Control Motor 1 to run to the desired position.

Step 2: After Motor1 reach the desired position, Motor2 begin to work, to act as a "disturbance" to pull Motor1 away from the desired position 15°. (The operating current of Motor2 is 1.6A which is greater than the operating current of Motor1, so the output torque of Motor2 is greater than the output torque of Motor1.)

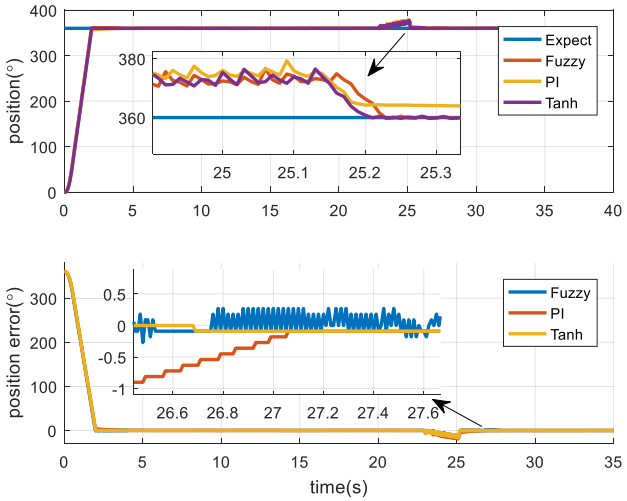

FIGURE 14. Step signal tracking with external disturbance results.

Step 3: Motor2 will stop after running 15° and enter the holding state, the holding current is 0.3A, at this time, because the operating current of Motor1 is 1A, the output torque is greater than the holding torque of Motor2, and Motor1 will drag the load to the desired position 360°.

Using the above testing strategy, three control algorithms are tested separately. The test results of three control algorithms are shown in Fig.14. From the disturbance test results, it can be seen that the dynamic performance of the Tanh controller is the best and the fastest recovery.

V. CONCLUSION

This paper solves the problem of closed-loop control of positions that do not require stepper motor models. This method is based on stepper motor pulse frequency control, a tanh algorithm is used in the position loop. The experiment results show that the proposed algorithm can improve both tracking accuracy and response performance. The algorithm does not need accurate mathematical model, and only has one parameter to be tuned, is easy to adjust parameters and use in engineering. At present, this method has been used in optical telescope dimming and focusing system, and has achieved good control performances. In the further study, tanh control method can be extended to the control of other types of motors.

REFERENCES

[1] P. Acarnley, *Stepping Motors: A Guide to Theory and Practice*. 2002.

[2] T. C. Krause and P. C. Krause, "Stepper motors," in *Introduction to Modern Analysis of Electric Machines and Drives*. Piscataway, NJ, USA: IEEE, 2023, pp. 211–237, doi: 10.1002/9781119908357.ch8.

[3] V. Groenhuis, G. Rolff, K. Bosman, L. Abelmann, and S. Stramigioli, "Multi-axis electric stepper motor," *IEEE Robot. Autom. Lett.*, vol. 6, no. 4, pp. 7201–7208, Oct. 2021, doi: 10.1109/LRA.2021.3097077.

[4] K. Eshaghi, Y. Li, Z. Kashino, G. Nejat, and B. Benhabib, "mROBerTO 2.0—An autonomous millirobot with enhanced locomotion for swarm robotics," *IEEE Robot. Autom. Lett.*, vol. 5, no. 2, pp. 962–969, Apr. 2020, doi: 10.1109/LRA.2020.2966411.

[5] S. V. Kumar, M. Mahesh, R. Palli, S. Shree, V. Jeshwanth, and V. Victor, "Study of stepper motor control using programmable logic controller (PLC) based on industry 4.0," in *Proc. Int. Conf. Smart Gener. Comput., Commun. Netw. (SMART GENCON)*, Bengaluru, India, Dec. 2022, pp. 1–4, doi: 10.1109/SMARTGENCON56628.2022.10083617.

[6] S. E. E. Rajan, C. H. Karthi, R. Ramya, and T. Anuradha, "Load based fuzzy controller for bipolar stepper motor," in *Proc. 4th Int. Conf. Inventive Res. Comput. Appl. (ICIRCA)*, Coimbatore, India, Sep. 2022, pp. 141–145, doi: 10.1109/ICIRCA54612.2022.9985770.

[7] Z. Li, "Robust control of PM spherical stepper motor based on neural networks," *IEEE Trans. Ind. Electron.*, vol. 56, no. 8, pp. 2945–2954, Aug. 2009, doi: 10.1109/TIE.2009.2023639.

[8] M. Defoort, F. Nollet, T. Floquet, and W. Perruquetti, "A third-order sliding-mode controller for a stepper motor," *IEEE Trans. Ind. Electron.*, vol. 56, no. 9, pp. 3337–3346, Sep. 2009, doi: 10.1109/TIE.2009.2026378.

[9] W. Kim, C. Yang, and C. C. Chung, "Design and implementation of simple field-oriented control for permanent magnet stepper motors without DQ transformation," *IEEE Trans. Magn.*, vol. 47, no. 10, pp. 4231–4234, Oct. 2011, doi: 10.1109/TMAG.2011.2157956.

[10] M. Bendjedia, Y. Ait-Amirat, B. Walther, and A. Berthon, "Position control of a sensorless stepper motor," *IEEE Trans. Power Electron.*, vol. 27, no. 2, pp. 578–587, Feb. 2012, doi: 10.1109/TPEL.2011.2161774.

[11] W. Kim, Y. Lee, D. Shin, and C. C. Chung, "Nonlinear gain position control using only position feedback for permanent magnet stepper motors," *IEEE Trans. Power Electron.*, vol. 36, no. 7, pp. 8506–8516, Jul. 2021, doi: 10.1109/TPEL.2020.3046849.

[12] S. Kim and C. K. Ahn, "Variable-performance positioning law for hybrid-type stepper motors via active damping injection and disturbance observer," *IEEE Trans. Circuits Syst. II, Exp. Briefs*, vol. 68, no. 4, pp. 1308–1312, Apr. 2021, doi: 10.1109/TCSII.2020.3020224.

[13] X. Li, W. Zhou, D. Jia, J. Qian, J. Luo, P. Jiang, and W. Ma, "A decoupling synchronous control method of two motors for large optical telescope," *IEEE Trans. Ind. Electron.*, vol. 69, no. 12, pp. 13405–13416, Dec. 2022, doi: 10.1109/TIE.2022.3142407.

[14] H. N. Tran, K. M. Le, and J. W. Jeon, "Adaptive current controller based on neural network and double phase compensator for a stepper motor," *IEEE Trans. Power Electron.*, vol. 34, no. 8, pp. 8092–8103, Aug. 2019, doi: 10.1109/TPEL.2018.2878928.

[15] K. M. Le, H. Van Hoang, and J. W. Jeon, "An advanced closed-loop control to improve the performance of hybrid stepper motors," *IEEE Trans. Power Electron.*, vol. 32, no. 9, pp. 7244–7255, Sep. 2017, doi: 10.1109/TPEL.2016.2623341.

[16] Y. Lee, D. Shin, W. Kim, and C. C. Chung, "Nonlinear $\mathcal{H}_2$ control for a nonlinear system with bounded varying parameters: Application to PM stepper motors," *IEEE/ASME Trans. Mechatronics*, vol. 22, no. 3, pp. 1349–1359, Jun. 2017, doi: 10.1109/TMECH.2017.2686901.

[17] F. Bernardi, E. Carfagna, G. Migliazza, G. Buticchi, F. Immovilli, and E. Lorenzani, "Performance analysis of current control strategies for hybrid stepper motors," *IEEE Open J. Ind. Electron. Soc.*, vol. 3, pp. 460–472, 2022, doi: 10.1109/OJIES.2022.3185659.

[18] M. Tobita and T. Matsuo, "Nonlinear model order reduction of a variable reluctance stepper motor using the parameterized Cauer ladder network method," *IEEE Trans. Magn.*, vol. 59, no. 5, pp. 1–4, May 2023, doi: 10.1109/TMAG.2022.3232701.

[19] O. Craiu, T. Ichim, and L. C. Popescu, "3D FEM model of a hybrid stepper using scalar-vector potential formulations," in *Proc. 13th Int. Symp. Adv. Topics Electr. Eng. (ATEE)*, Bucharest, Romania, Mar. 2023, pp. 1–5, doi: 10.1109/ATEE58038.2023.10108283.

[20] K. Balakrishnan, B. Umamaheswari, and K. Latha, "Identification of resonance in hybrid stepper motor through measured current dynamics in online for accurate position estimation and control," *IEEE Trans. Ind. Informat.*, vol. 9, no. 2, pp. 1056–1063, May 2013, doi: 10.1109/TII.2012.2221722.

[21] M. Tao, S. Wang, H. Chen, H. Pan, J. Shi, and Y. Zhang, "Information space of sensor networks: Lagrangian, energy-momentum tensor, and applications," *Chin. J. Aeronaut.*, vol. 36, no. 3, pp. 271–284, Mar. 2023, doi: 10.1016/j.cja.2022.09.006.

[22] M. Butcher, A. Masi, R. Picatoste, and A. Giustiniani, "Hybrid stepper motor electrical model extensions for use in intelligent drives," *IEEE Trans. Ind. Electron.*, vol. 61, no. 2, pp. 917–929, Feb. 2014, doi: 10.1109/TIE.2013.2254097.

[23] M. Tao, S. Wang, H. Chen, and X. Wang, "Information space of multi-sensor networks," *Inf. Sci.*, vol. 565, pp. 128–145, Jul. 2021, doi: 10.1016/j.ins.2021.02.059.

[24] S. Ajdukovic, B. Kuzmanovic, and P. Crnosija, "Microcomputer implementation of optimal algorithms for closed-loop control of hybrid stepper motor drives," *IEEE Trans. Ind. Electron.*, vol. 47, no. 6, pp. 1319–1325, Dec. 2000, doi: 10.1109/41.887960.

[25] S. Kim and C. K. Ahn, "Position regulator with variable cut-off frequency mechanism for hybrid-type stepper motors," *IEEE Trans. Circuits Syst. I, Reg. Papers*, vol. 67, no. 10, pp. 3533–3540, Oct. 2020, doi: 10.1109/TCSI.2020.2988044.

[26] W. Kim, D. Shin, and C. C. Chung, "Microstepping with nonlinear torque modulation for permanent magnet stepper motors," *IEEE Trans. Control Syst. Technol.*, vol. 21, no. 5, pp. 1971–1979, Sep. 2013, doi: 10.1109/TCST.2012.2211079.

[27] W. Kim, D. Shin, and C. C. Chung, "Microstepping using a disturbance observer and a variable structure controller for permanent-magnet stepper motors," *IEEE Trans. Ind. Electron.*, vol. 60, no. 7, pp. 2689–2699, Jul. 2013, doi: 10.1109/TIE.2012.2198033.

[28] D. Shin, W. Kim, Y. Lee, and C. C. Chung, "Phase-compensated microstepping for permanent-magnet stepper motors," *IEEE Trans. Ind. Electron.*, vol. 60, no. 12, pp. 5773–5780, Dec. 2013, doi: 10.1109/TIE.2013.2238879.

[29] D. R. Gaan, M. Kumar, and S. Sudhakar, "Real-time precise position tracking with stepper motor using frequency modulation based microstepping," *IEEE Trans. Ind. Appl.*, vol. 54, no. 1, pp. 693–701, Jan./Feb. 2018, doi: 10.1109/TIA.2017.2753158.

[30] J. Pillans, "Reducing position errors by vibration optimization of stepper motor drive waveforms," *IEEE Trans. Ind. Electron.*, vol. 68, no. 6, pp. 5176–5183, Jun. 2021, doi: 10.1109/TIE.2020.2982123.

[31] Y.-L. Huang, C.-H. Liang, B.-H. Chen, and C.-C. Lan, "Torque-sensorless control of stepper motors for low-cost compliant motion generation," *IEEE Access*, vol. 9, pp. 94495–94504, 2021, doi: 10.1109/ACCESS.2021.3094506.

[32] M. Bodson, J. S. Sato, and S. R. Silver, "Spontaneous speed reversals in stepper motors," *IEEE Trans. Control Syst. Technol.*, vol. 14, no. 2, pp. 369–373, Mar. 2006, doi: 10.1109/TCST.2005.863675.

[33] R. D. A. Maravi, O. G. M. Iparraguirre, and G. S. R. Prado, "Implementation of a digital PID control for the compensation of loss steps from CORE XY 3D printer motors working at high speeds," in *Proc. IEEE ANDESCON*, Quito, Ecuador, Oct. 2020, pp. 1–6, doi: 10.1109/ANDESCON50619.2020.9272178.

[34] L. Zhou, S. Yang, and X. Gao, "Modeling of stepper motor control system and running curve simulation," *Electr. Mach. Control*, vol. 15, no. 1, pp. 20–25, Jan. 2011, doi: 10.15938/j.emc.2011.01.015.

[35] B. Wang, Q. Liu, L. Zhou, L. Bu, X. Li, and J. Zhang, "Modeling of stepper motor control system and optimization of acceleration and deceleration curve," *Electr. Mach. Control*, vol. 22, no. 1, pp. 37–42, Jan. 2018, doi: 10.15938/j.emc.2018.01.006.

[36] E. Normanyo, O. R. Agyare, and R. A. Rashid, "MATLAB implementation of position control of a hybrid stepper motor using fuzzy logic controller," in *Proc. IEEE AFRICON*, Accra, Ghana, Sep. 2019, pp. 1–8, doi: 10.1109/AFRICON46755.2019.9134047.

[37] J. Shi, J. Chen, and W. Qi, "Research on stepper motor servo controller based on pan-Boolean PID control," in *Proc. 39th Chin. Control Conf. (CCC)*, Shenyang, China, Jul. 2020, pp. 2686–2690, doi: 10.23919/CCC50068.2020.9189307.

WENLIN ZHOU received the B.S. and M.S. degrees from the School of Automation, Northwestern Polytechnical University, China, in 2012 and 2015, respectively. She is currently a Research Associate with the Institute of Optics and Electronics (IOE), Chinese Academy of Sciences (CAS), China. Her research interests include robust control, ADRC, PMSM, and motion control systems.

XIN LI received the B.S. and M.S. degrees from the School of Automation, Northwestern Polytechnical University, China, in 2011 and 2014, respectively, and the Ph.D. degree from the Institute of Optics and Electronics (IOE), Chinese Academy of Sciences (CAS), China, in 2020. His research interests include robust control, ADRC, and high precision servo control system in large photoelectric telescopes.

JUNZHANG QIAN received the B.S. degree from the School of Automation, Northwestern Polytechnical University, China, in 2012, and the Ph.D. degree from the Institute of Optics and Electronics (IOE), Chinese Academy of Sciences (CAS), China, in 2017. He is a Research Associate with IOE. His research interests include PMSM, sliding mode control (SMC), and robust control.

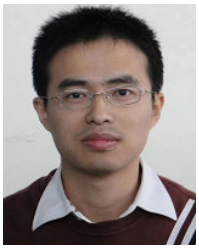

MO XIA received the B.S. degree from Wuhan University, Wuhan, China, and the M.S. degree from the University of Science and Technology of China, China. He is an Associate Researcher with the Institute of Optics and Electronics (IOE), Chinese Academy of Sciences (CAS), China. His research interests include photoelectric detection, automation control, and large photoelectric telescope.

YI PU received the B.S. degree from Sichuan Normal University, Chengdu, China, and the M.S. degree from the University of Science and Technology of China, China. He is an Associate Researcher and a Master's Supervisor with the Institute of Optics and Electronics (IOE), Chinese Academy of Sciences (CAS), China. His main research interests include the overall technology of photoelectric telescopes, the overall design of automation control, and system integration.

PING JIANG graduated from the Sichuan University of China. He is a Research Fellow with the Institute of Optics and Electronics (IOE), Chinese Academy of Sciences (CAS), China. His research interests include photoelectric detection, precision machinery, and photoelectric telescope.

JINLONG HUANG received the Ph.D. degree from the University of Electronic Science and Technology of China. He is a Research Fellow with the Institute of Optics and Electronics (IOE), Chinese Academy of Sciences (CAS), China. His research interests include photoelectric detection, precision machinery, and large photoelectric telescope.